

## **Supporting Information**

Anhydrous Amorphous Calcium Carbonate (ACC) is  
Structurally Different from the Transient Phase of Biogenic  
ACC

## Experimental Methods

**Sample Preparation.** All chemicals were obtained from Acros and used as received without further purification. For the calcite prepared by direct mixing, 25 mL of  $(\text{NH}_4)_2\text{CO}_3$  (0.2 M, pH 8.75) was added into 25 mL of  $\text{CaCl}_2$  (0.2 M, pH 9), followed by aging at room temperature for 4 hours. The sample collected was lyophilized and stored in desiccator. The ACC samples were prepared as follows. A stock solution of carbonate was prepared by mixing 10 mL of  $(\text{NH}_4)_2\text{CO}_3$  (0.2 M) and 10 mL of ammonia solution (1 M). An aliquot of 5 mL of the carbonate solution was rapidly mixed with 5 mL of  $\text{CaCl}_2$  (0.1 M) at 4 °C. The precipitate was collected immediately with polycarbonate filter membrane (0.2  $\mu\text{m}$ , Whatman) and washed with cold anhydrous ethanol three times, followed by lyophilization.

**Sample Characterization.** Scanning electron microscopy (SEM) images were taken on a JEOL JSM-7600F field emission scanning electron microscope. Transmission electron microscope (TEM) images were taken on a JOEL JEM-2100F Field Emission Electron Microscope operating at 200 kV. X-Ray powder diffraction (XRD) analyses were performed on a PANalytical X'Pert PRO diffractometer using  $\text{Cu-K}\alpha$  radiation ( $\lambda = 1.5418 \text{ \AA}$ ). FT-IR measurements were conducted on a Nicolet IS5 FT-IR Spectrometer (Thermo Scientific). For the thermogravimetric analysis (TGA) and Differential scanning calorimetry (DSC), the samples were heated in a Mettler Toledo DSC/TGA STARe system from 313 K to 1073 K at a ramping rate of 10 K/min with  $\text{N}_2$  purging (50 mL/min).

**Synchrotron based characterization techniques.** XRD and soft X-ray spectroscopy measurements were respectively carried out in BL01C2 and BL24A beamlines of Taiwan Light Source (TLS) of National Synchrotron Radiation Research Center

(NSRRC). TLS is a 1.5 GeV ring operated in a top-up injection mode with a constant ring current of 360 mA. For the XRD measurements, the wavelength of the incident X-rays was 0.68881 Å (18 keV) and the X-ray beam was collimated to a typical dimension of 0.5 mm × 0.5 mm (H × V) at the sample position. The diffraction pattern was recorded with a Mar345 imaging plate detector positioned approximately 430 mm from the sample, which was packed into a 0.5 mm capillary, with a typical exposure duration of 60 s. The one-dimensional powder diffraction profile was converted by cake-type integration with GSAS II.<sup>[1]</sup> The diffraction angles were calibrated by the Bragg positions of the LaB<sub>6</sub> standard.

Ca L-edge NEXAFS spectra were acquired from a newly constructed APXPS end-station composed of a 4-stage differentially-pumped electron energy analyzer (Phoibos NAP 150, SPECS GmbH) for XPS measurements, a preparation chamber equipped with a load-lock sample transfer, and a gas-manifold. The set-up pertinent to the present measurements is depicted in Figure S1. X-ray from the beamline passes through a Si<sub>3</sub>N<sub>4</sub> membrane window, that serves to isolate the UHV beamline from the analysis chamber, and impinges on the sample at a fixed 55° from the sample surface normal with an X-ray footprint of 0.3 mm (V) × 1.2 mm (H). The water vapor was admitted into the chamber via a precision leak valve. The sample was heated by a near IR laser striking the back side of the sample with the sample temperature regulated by a PID controller. The Ca L-edge NEXAFS spectra were acquired by measuring the sample drain current in the so-called total electron yield (TEY) detection mode from 340 to 360 eV at an incremental energy step of 0.1 eV. The probing depth of TEY mode in soft X-ray photon energy range is usually quoted as a few tens of nm. Calcium carbonate material has an indirect energy gap of 6 eV and the sample charging problem during XPS and XAS measurements were minimized by working

on the sample region of presumably smaller thickness where spectral shift due to charging is lessened or even eliminated. For the measurements where ACC was exposed to water vapor of mbar pressure, the presence of gas-phase charged species near the sample, a unique attribute of APXPS technique, further alleviated the charging problem.

**Spectral Deconvolution.** All the NEXAFS spectra were fitted with a commercial software Unifit 2018. For the fitting of Ca *L* edge spectra, the background was composed of a linear offset plus two step functions corresponding to the transitions to  $L_3$  and  $L_2$  continua with the most suitable step edge locations determined to be at 349.3 and 352.5 eV, close to the edge locations of 349.5 and 352.5 eV given by Politi et al.<sup>[2]</sup> On top of the background, a set of four Voigt functions were employed to represent two spin-orbit split components with each further split into two by crystal field splitting. Gaussian components of the Voigt function were chosen to be at least nearly the same because of the same instrument broadening contribution and similar sample homogeneity.

## FIGURES

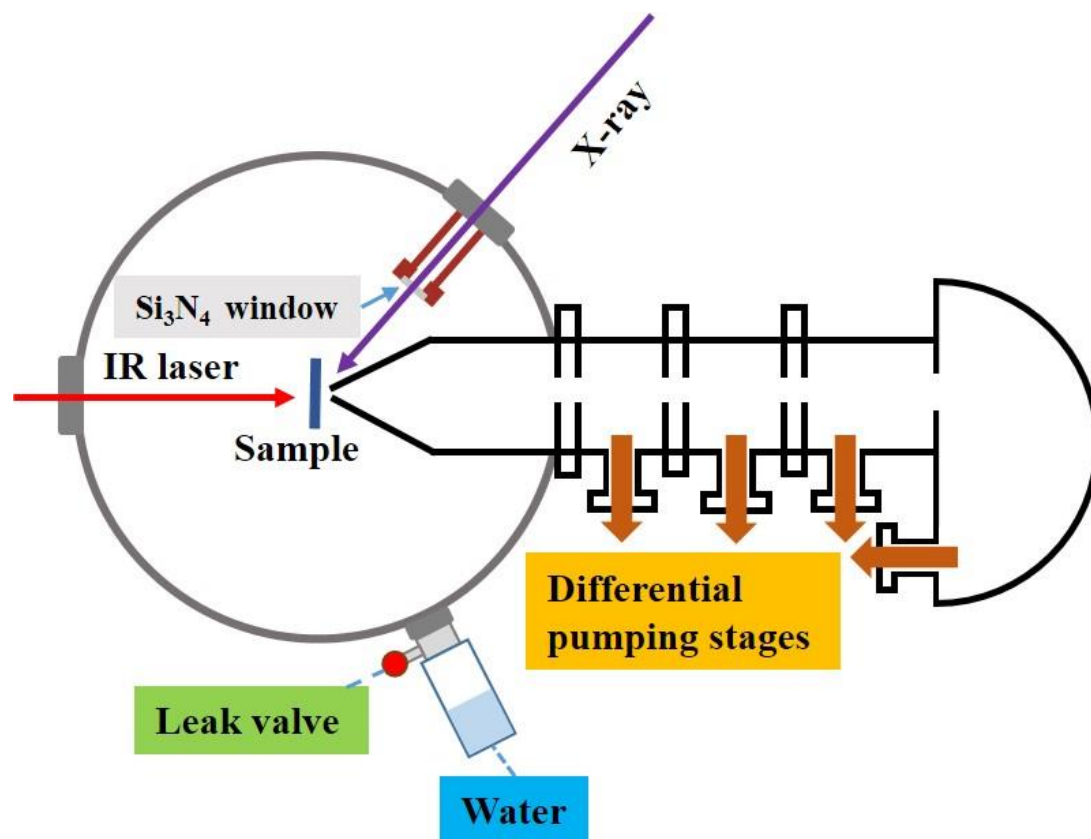


Figure S1. Schematic illustration of APXPS experimental setup relevant to present in-situ Ca *L*-edge NEXAFS measurements.

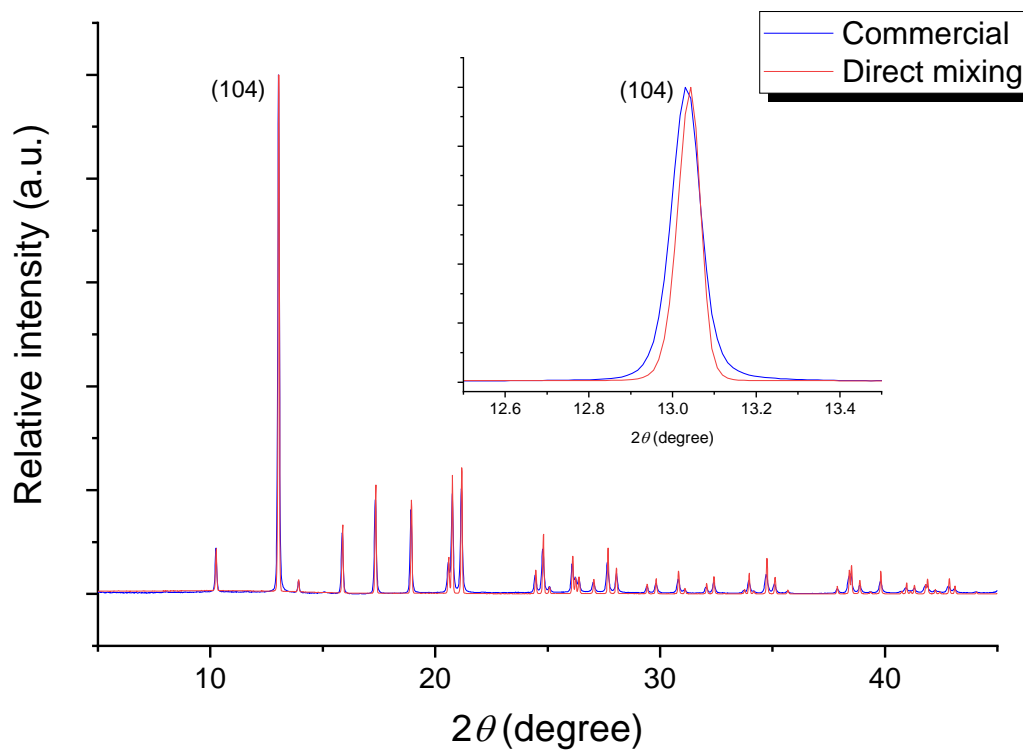
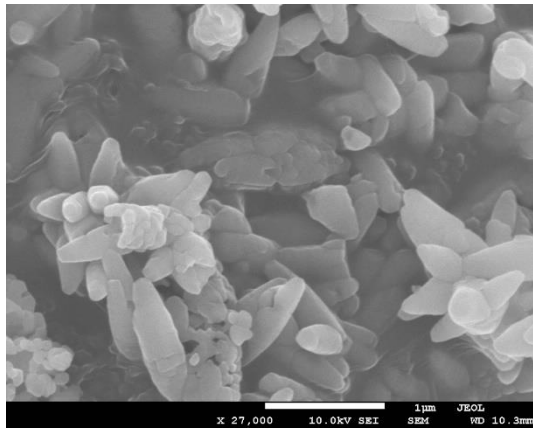
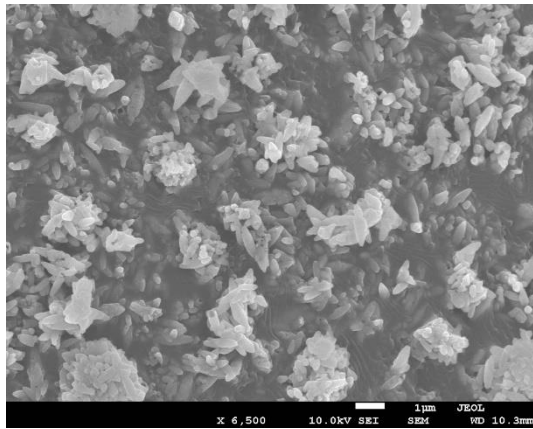


Figure S2. XRD diffractograms of commercial calcite (Acros) and the calcite sample prepared by direct mixing (see the main text) were acquired at NSRRC. The inset highlights the (104) diffraction peaks, where the peak width of the commercial sample was larger than that of the synthetic sample.

Commercial calcite (Acros)



Synthetic calcite

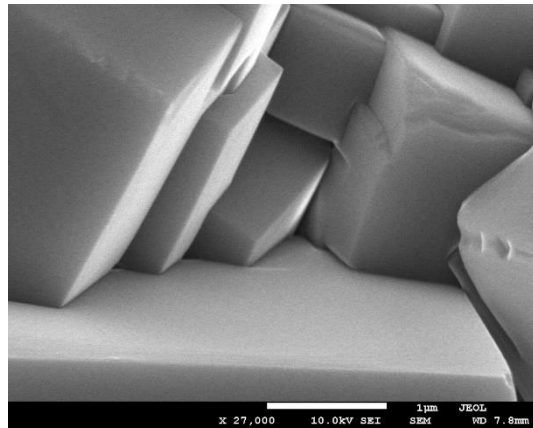
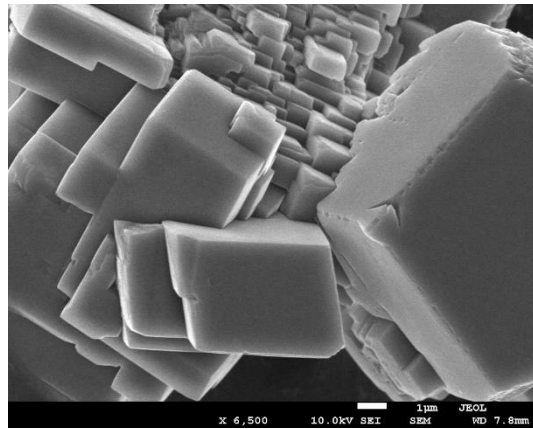


Figure S3. SEM images of commercial calcite (left panels) and synthetic calcite (right panels).

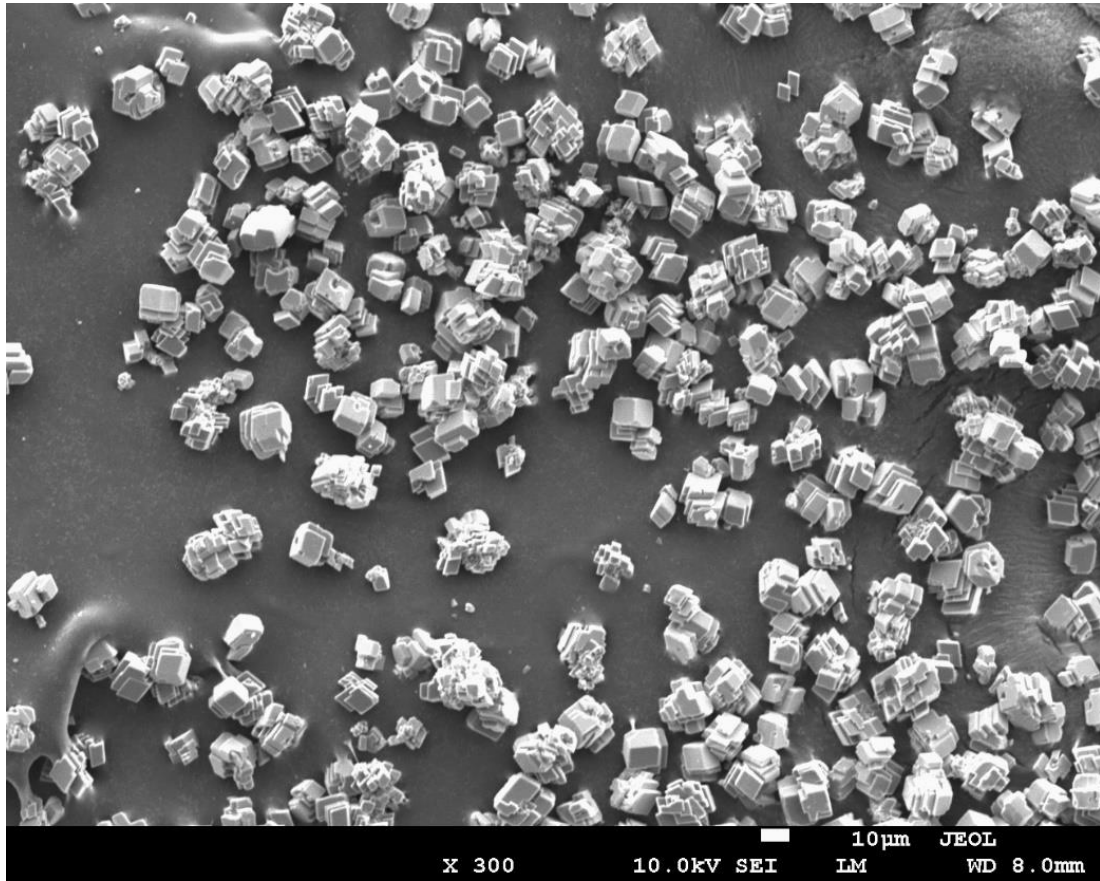


Figure S4. SEM image of the synthetic calcite.

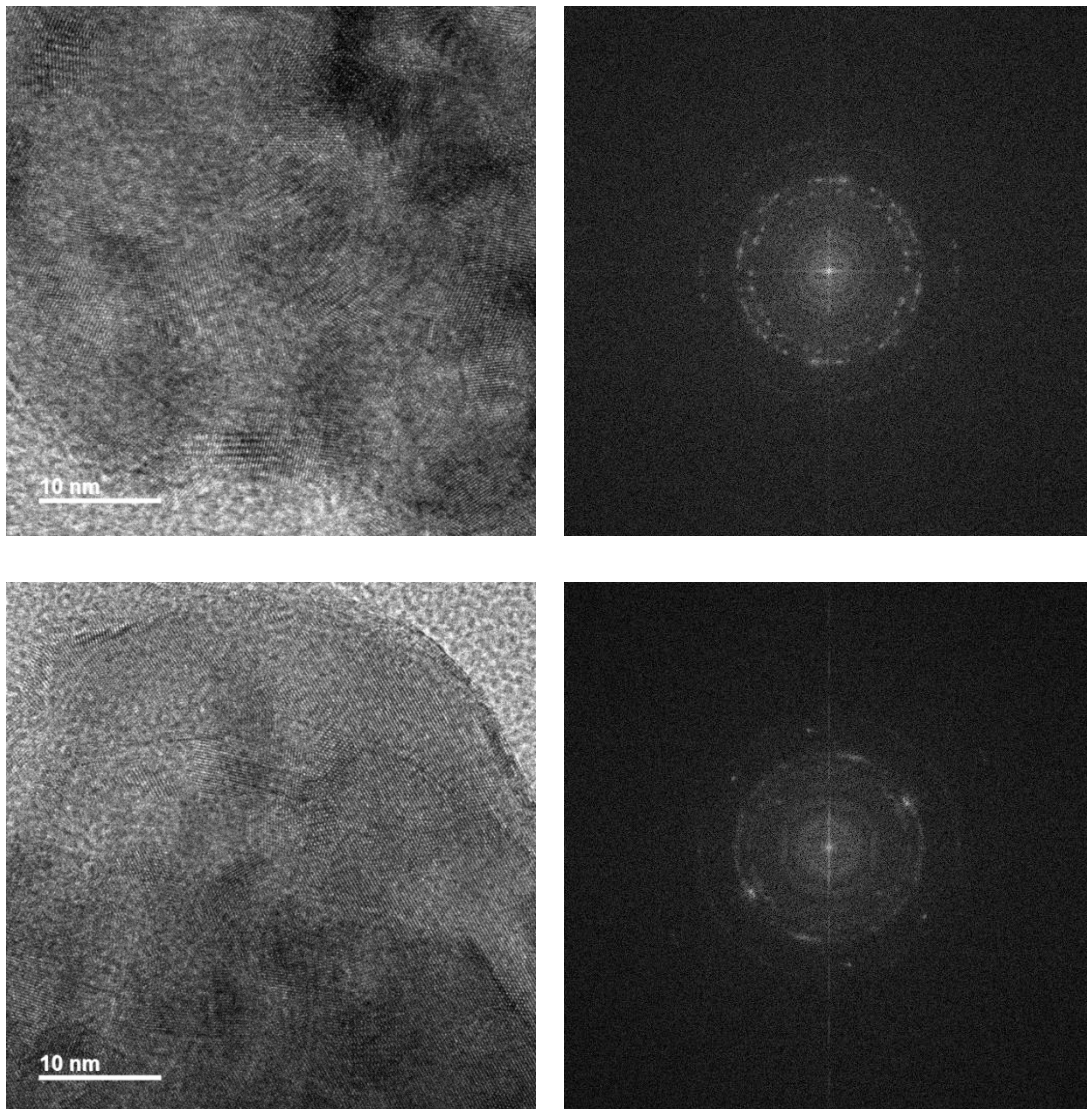


Figure S5. TEM images of commercial calcite. The FFT of the high-resolution TEM images were shown on the right, which indicated that the commercial calcite was polycrystalline at the nanometer scale.

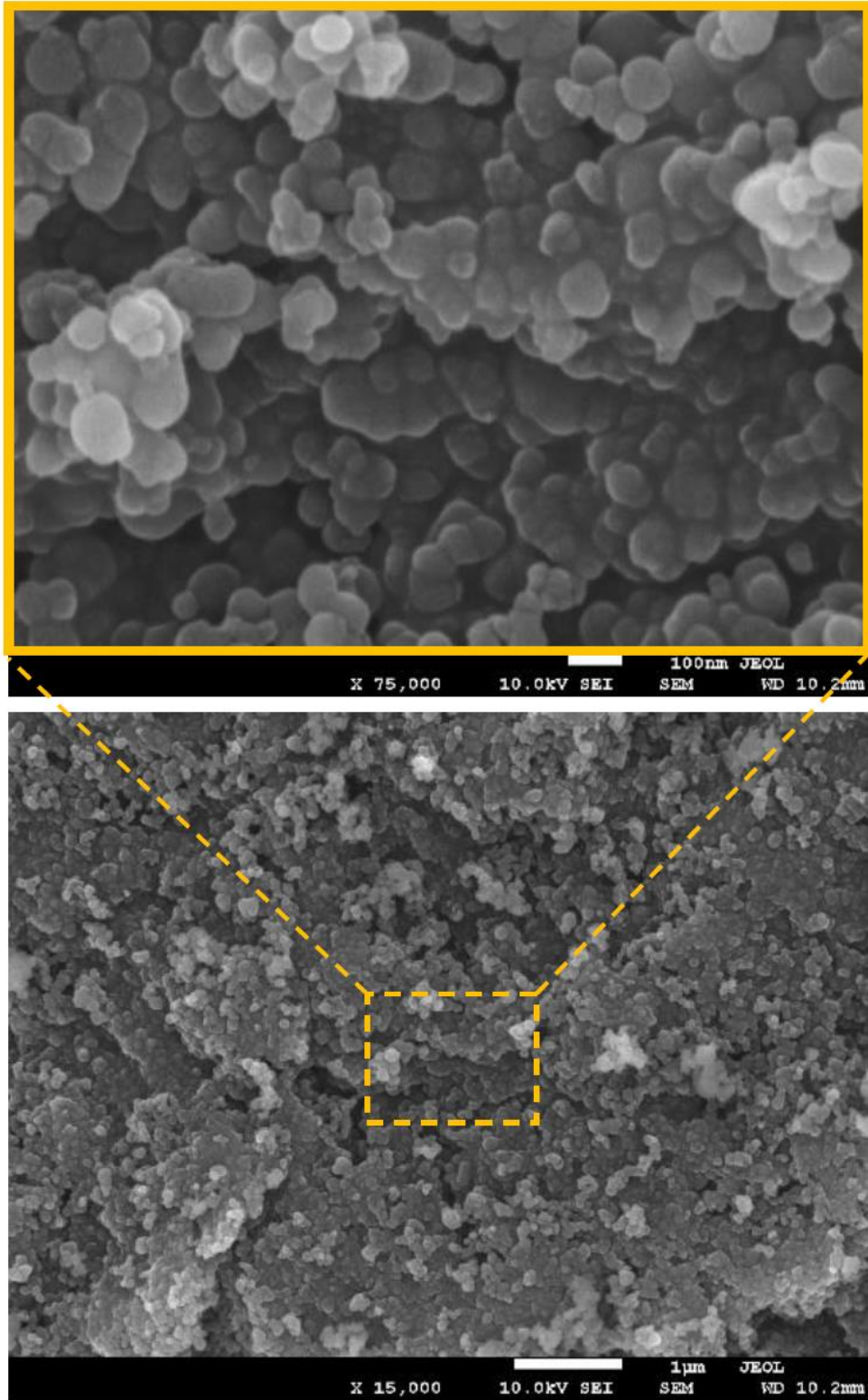


Figure S6. SEM images of the hydrated ACC sample.

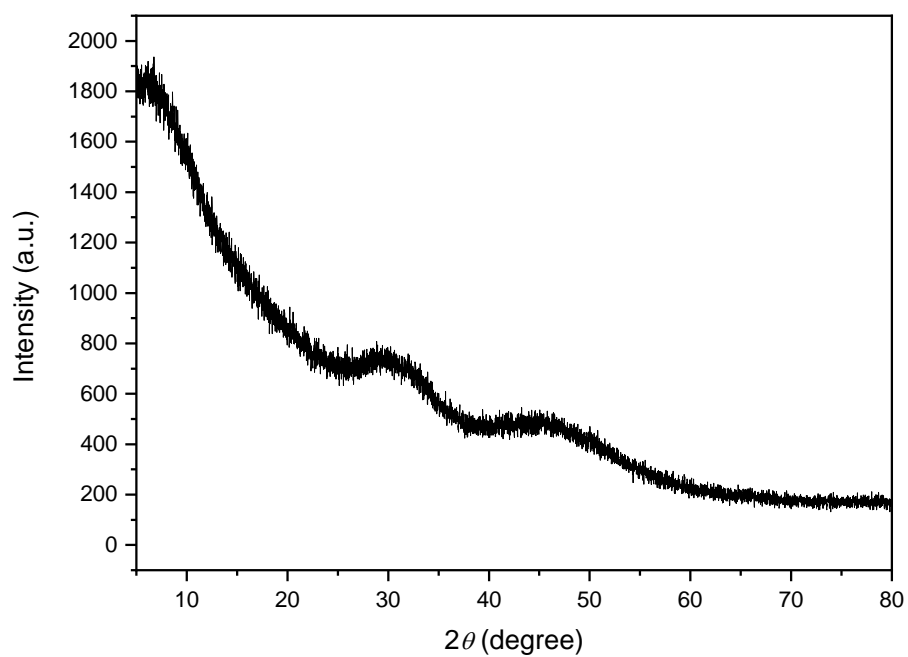


Figure S7. XRD diffractogram of the hydrated ACC sample acquired by in-house XRD facility.

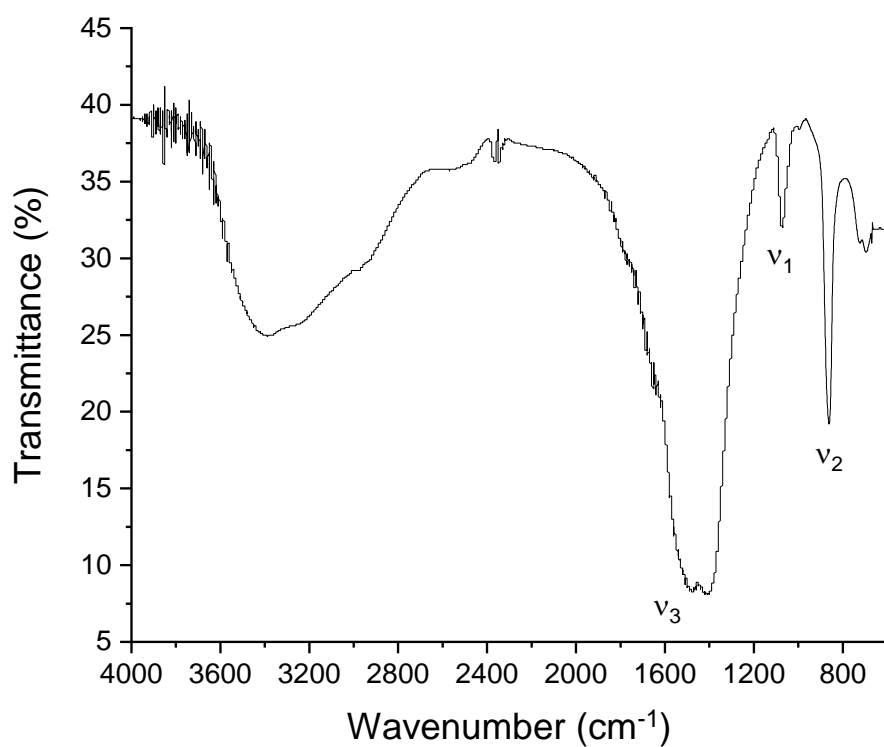


Figure S8. FT-IR spectrum of the hydrated ACC sample. The peaks at 1072 cm<sup>-1</sup> were assigned to the symmetric stretching of carbonate ( $\nu_1$ ); 862 cm<sup>-1</sup> to the out-of-plane bending ( $\nu_2$ ); 1496 and 1475 cm<sup>-1</sup> to the asymmetric stretching ( $\nu_3$ ).

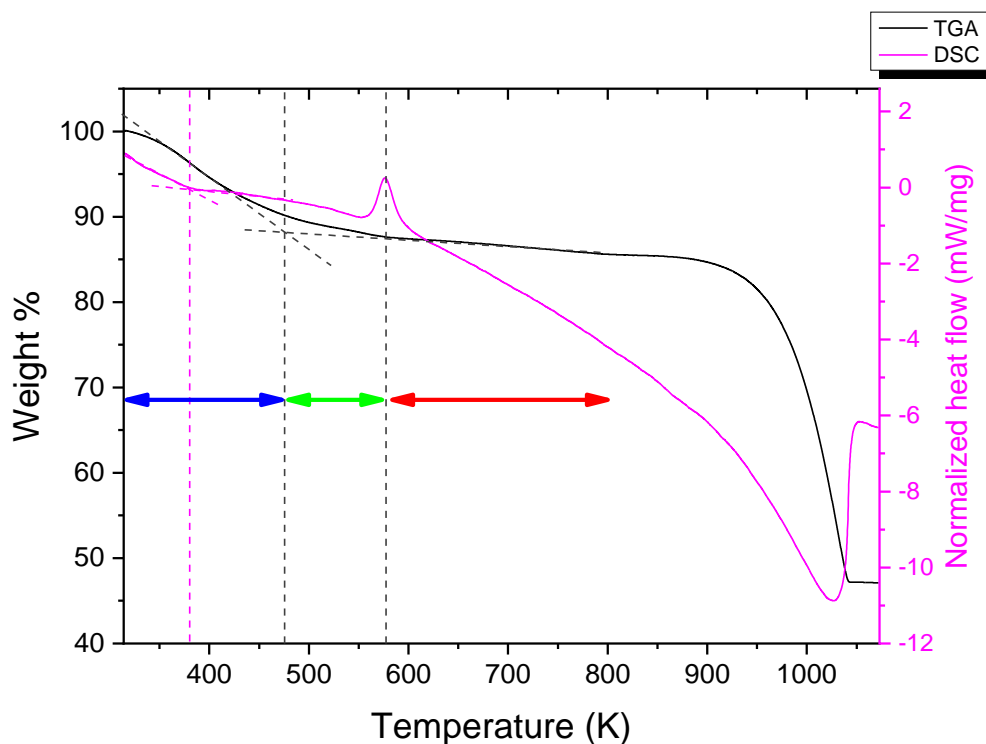


Figure S9. TGA and DSC results of the hydrated ACC sample. The dehydration of process was largely completed at 470 K, whereas the crystallization of the anhydrous ACC occurred at 578 K. Thus, the sample in the temperature regions highlighted in blue and green arrows correspond to hydrated and anhydrous ACC, respectively. The red arrow indicated the region at which the anhydrous ACC sample would be transformed to calcite. At around 900 K, calcite gradually decomposed into CaO and CO<sub>2</sub>. From the DSC curve, we assumed that loosely bound water was completely removed at 380 K. From the weight loss, the molecular formula of the hydrated ACC was determined as follows:

Total water content

Weight % at 1073 K (CaO)	Calculated weight % of CaCO <sub>3</sub>	Total water content	Water per formula unit
47.1%	84.1%	15.9%	CaCO <sub>3</sub> ·1.05H <sub>2</sub> O

Tightly bound water content

Weight % at 380 K	Loosely bound water	Total water content	Tightly bound water content	Tightly bound water per formula unit
93.2%	6.8%	15.9%	9.1%	CaCO <sub>3</sub> ·0.60H <sub>2</sub> O

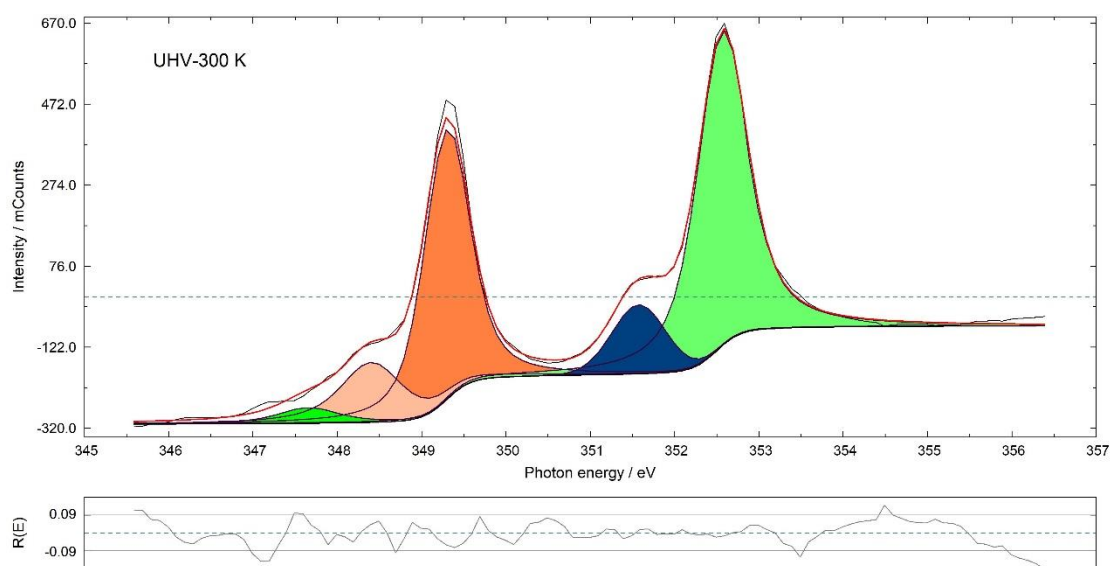


Figure S10. Ca  $L_{2,3}$ -edge NEXAFS spectra of amorphous calcium carbonate acquired at 300 K under ultra-high vacuum conditions.

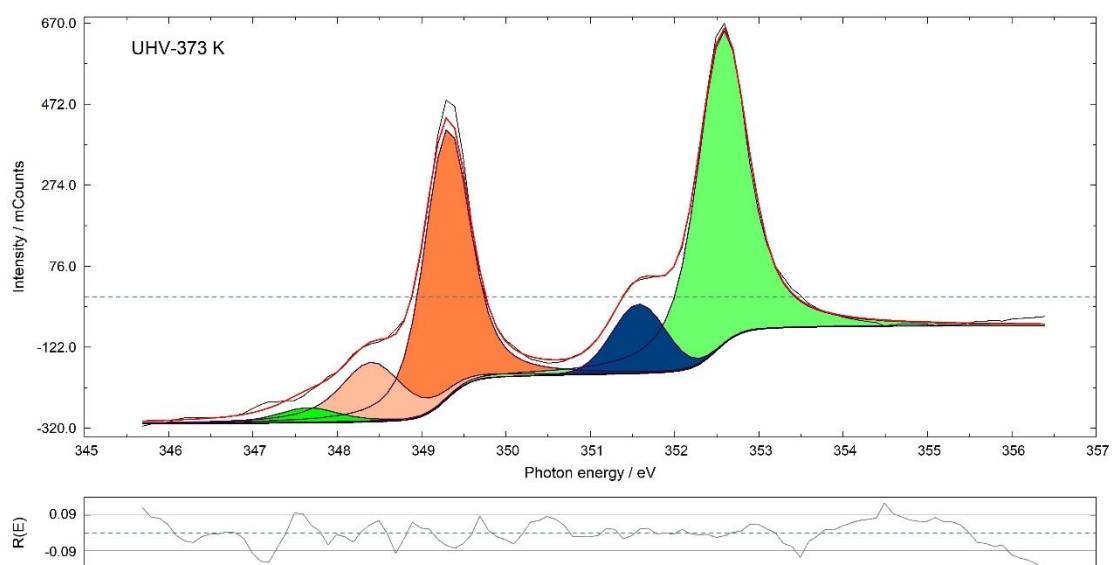


Figure S11. Ca  $L_{2,3}$ -edge NEXAFS spectra of amorphous calcium carbonate acquired at 373 K under ultra-high vacuum conditions.

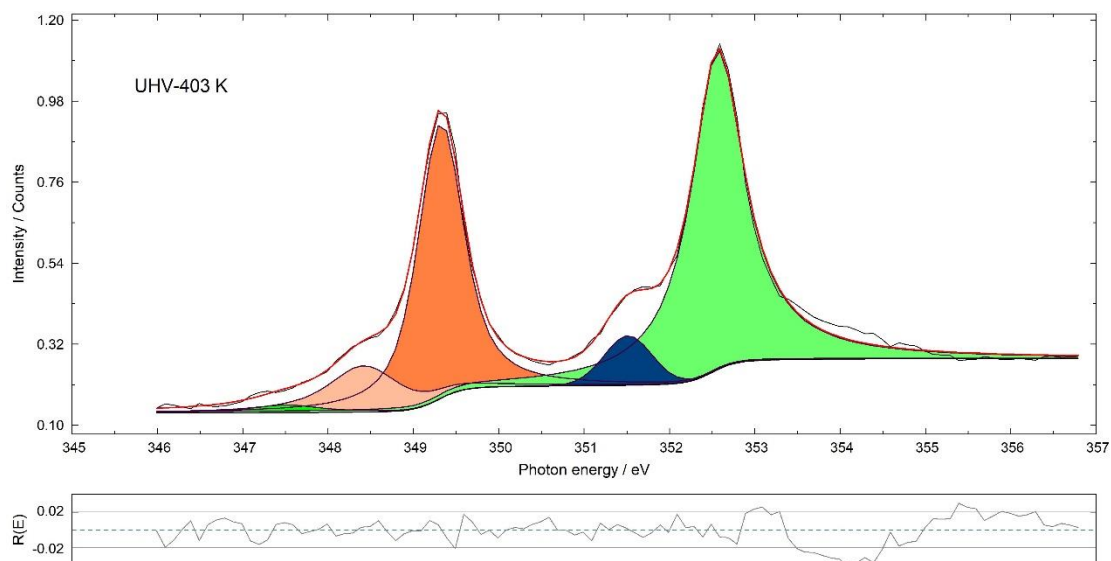


Figure S12. Ca  $L_{2,3}$ -edge NEXAFS spectra of amorphous calcium carbonate acquired at 403 K under ultra-high vacuum conditions.

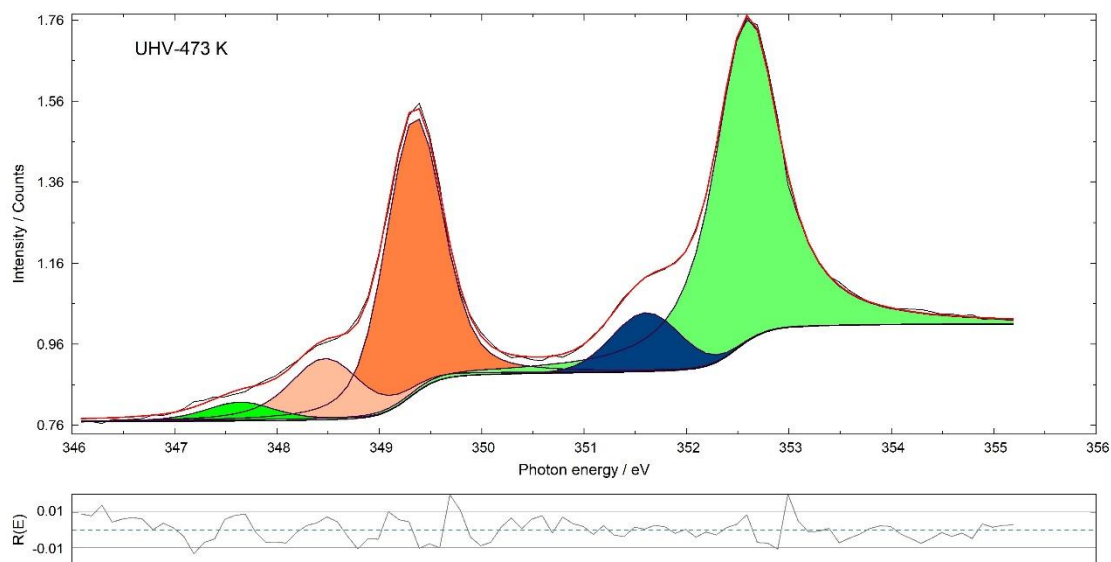


Figure S13. Ca  $L_{2,3}$ -edge NEXAFS spectra of amorphous calcium carbonate acquired at 473 K under ultra-high vacuum conditions.

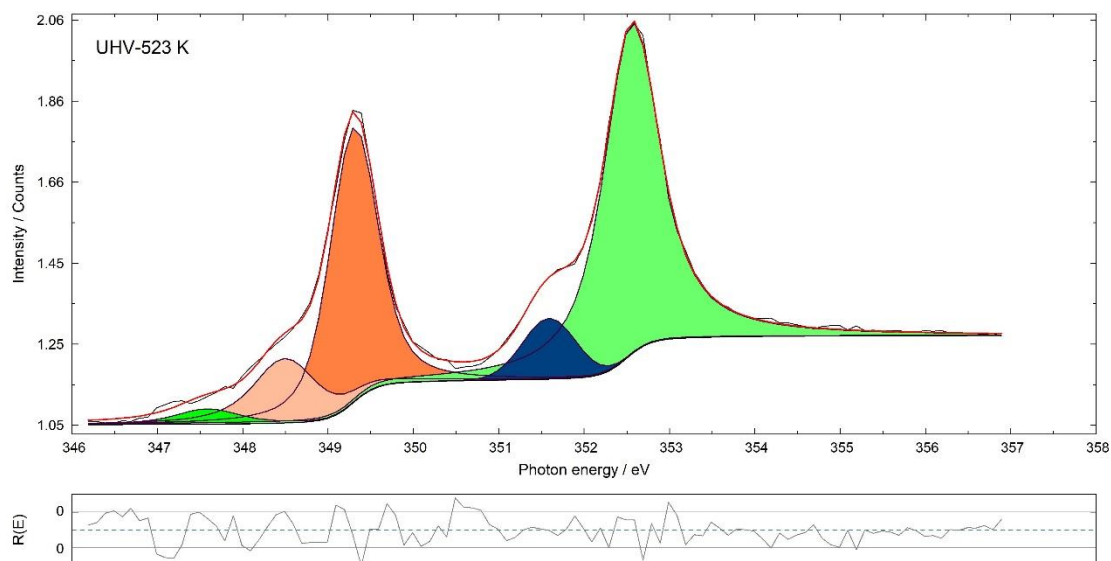


Figure S14. Ca  $L_{2,3}$ -edge NEXAFS spectra of amorphous calcium carbonate acquired at 523 K under ultra-high vacuum conditions.

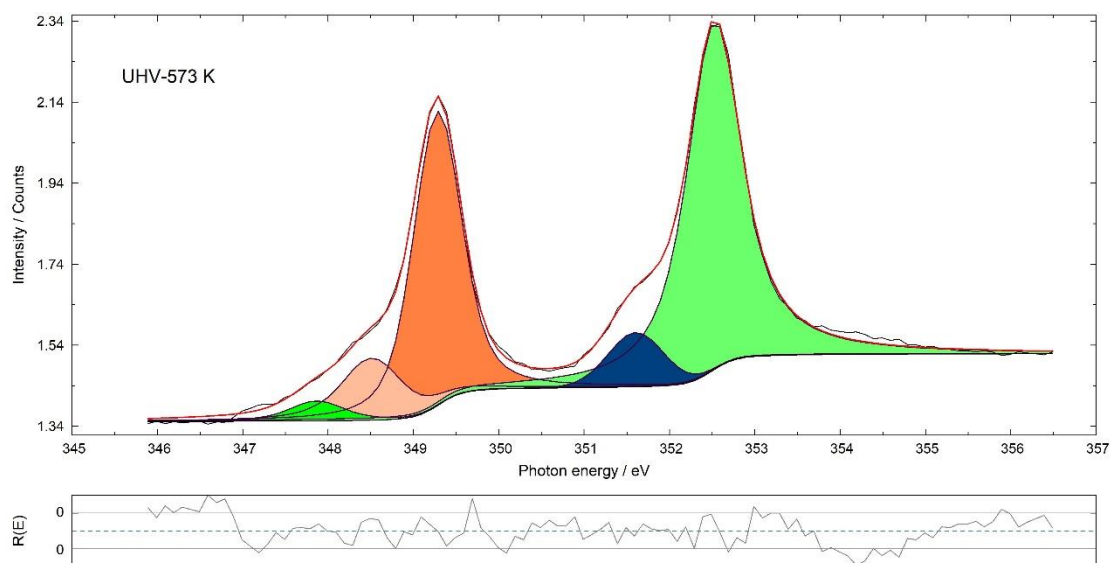


Figure S15. Ca  $L_{2,3}$ -edge NEXAFS spectra of amorphous calcium carbonate acquired at 573 K under ultra-high vacuum conditions.

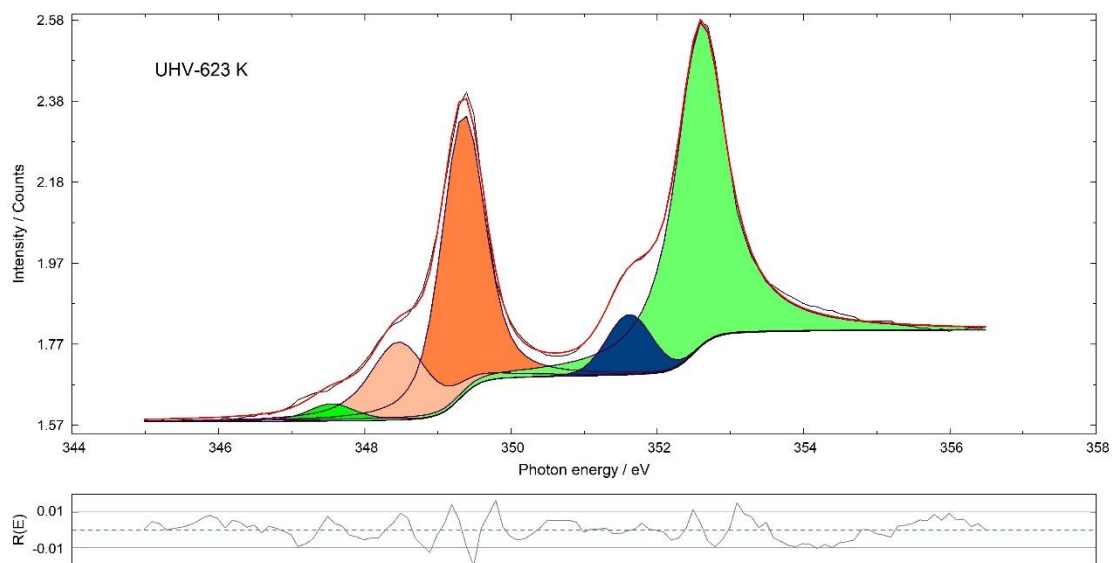


Figure S16. Ca  $L_{2,3}$ -edge NEXAFS spectra of amorphous calcium carbonate acquired at 623 K under ultra-high vacuum conditions.

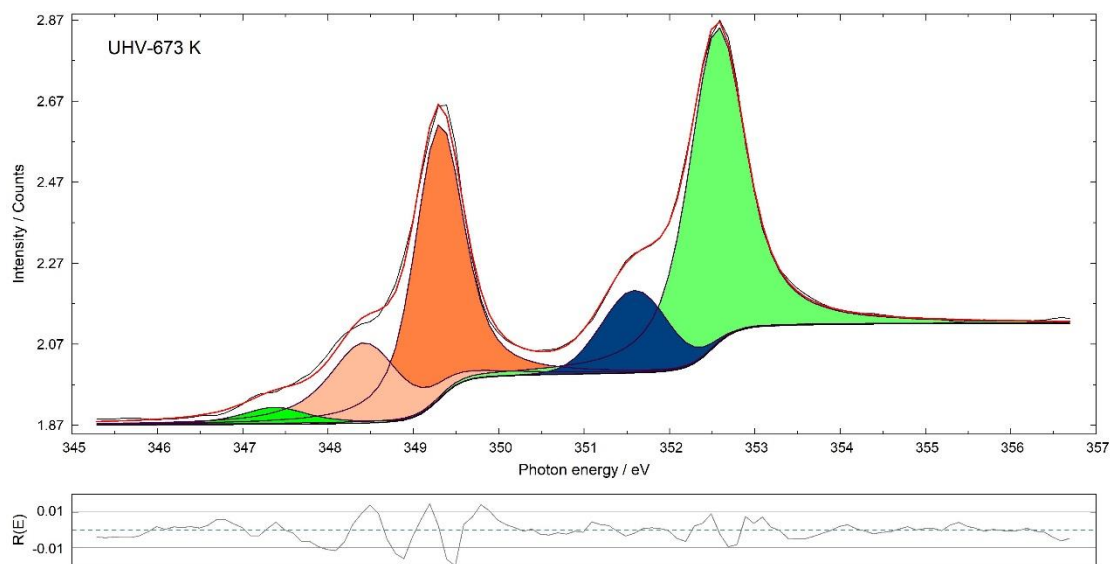


Figure S17. Ca  $L_{2,3}$ -edge NEXAFS spectra of amorphous calcium carbonate acquired at 673 K under ultra-high vacuum conditions.

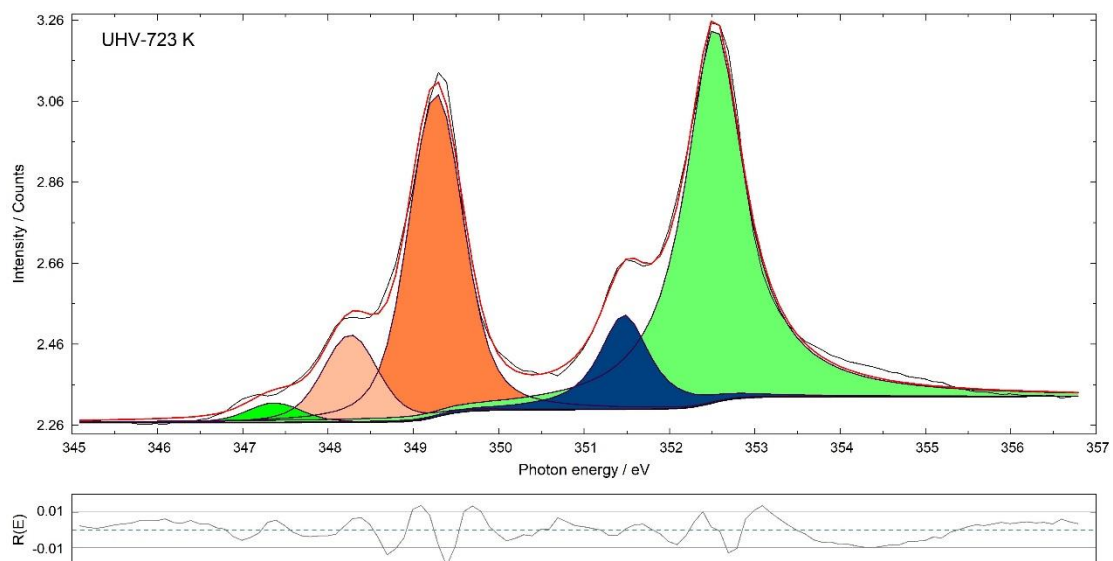


Figure S18. Ca  $L_{2,3}$ -edge NEXAFS spectra of amorphous calcium carbonate acquired at 723 K under ultra-high vacuum conditions.

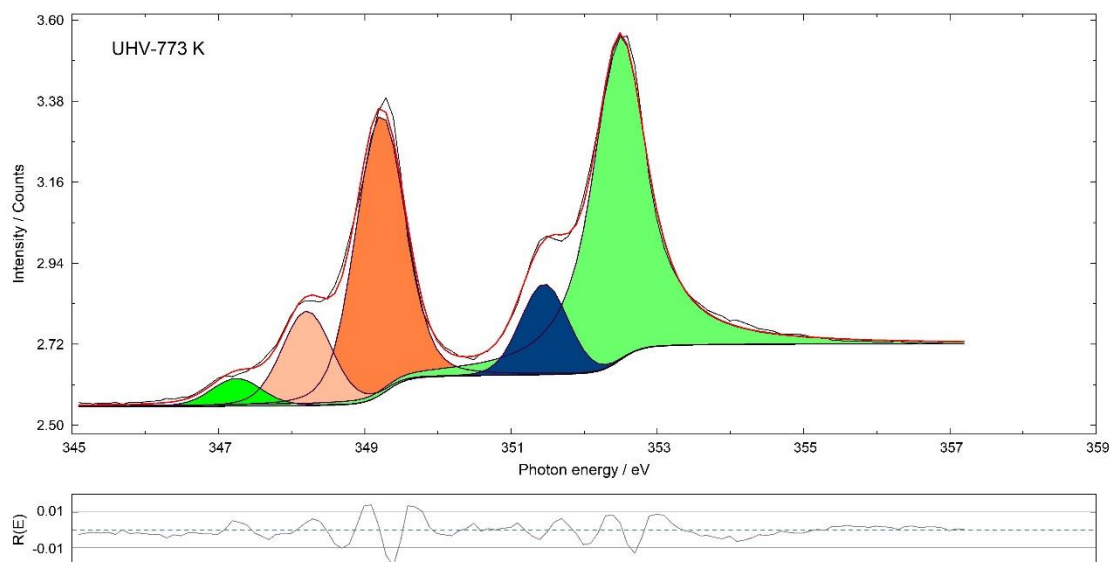


Figure S19. Ca  $L_{2,3}$ -edge NEXAFS spectra of amorphous calcium carbonate acquired at 773 K under ultra-high vacuum conditions.

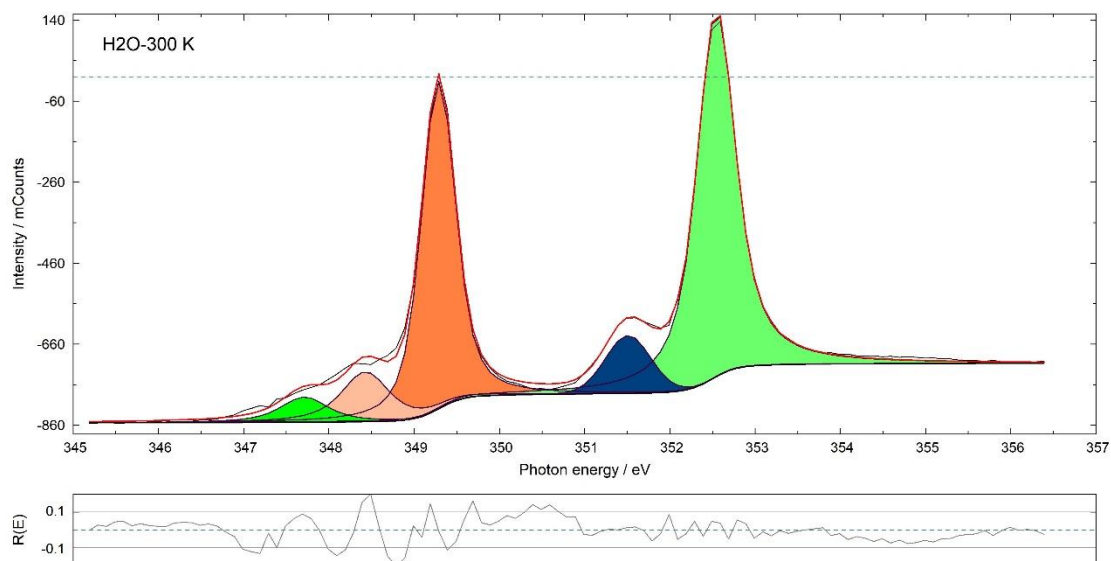


Figure S20. Ca  $L_{2,3}$ -edge NEXAFS spectra of amorphous calcium carbonate acquired at 300 K under an atmosphere of 0.4 mbar of water vapor (relative humidity 1.3%).

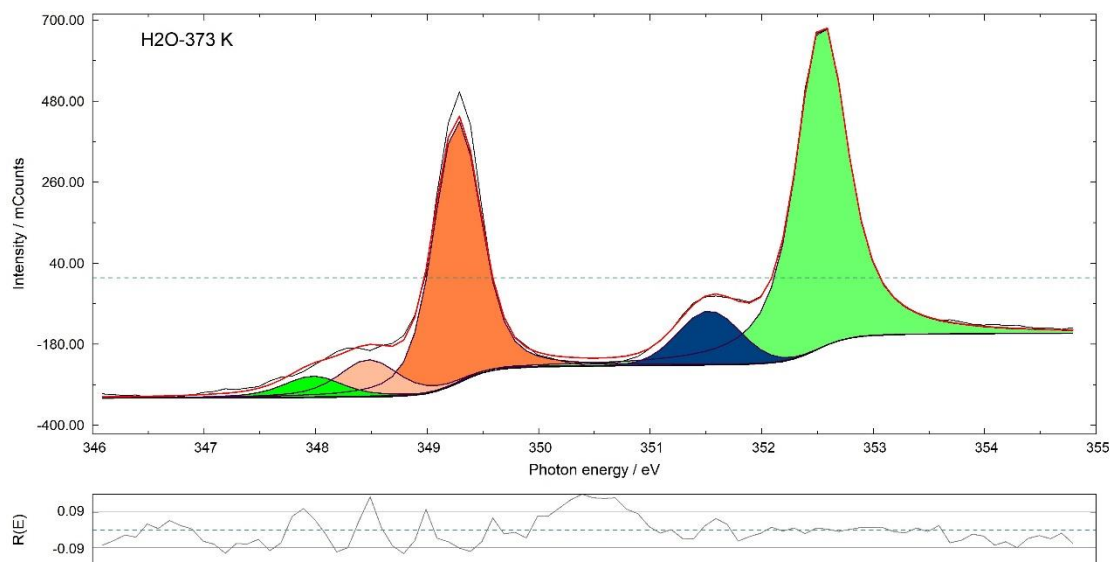


Figure S21. Ca  $L_{2,3}$ -edge NEXAFS spectra of amorphous calcium carbonate acquired at 373 K under an atmosphere of 0.4 mbar of water vapor.

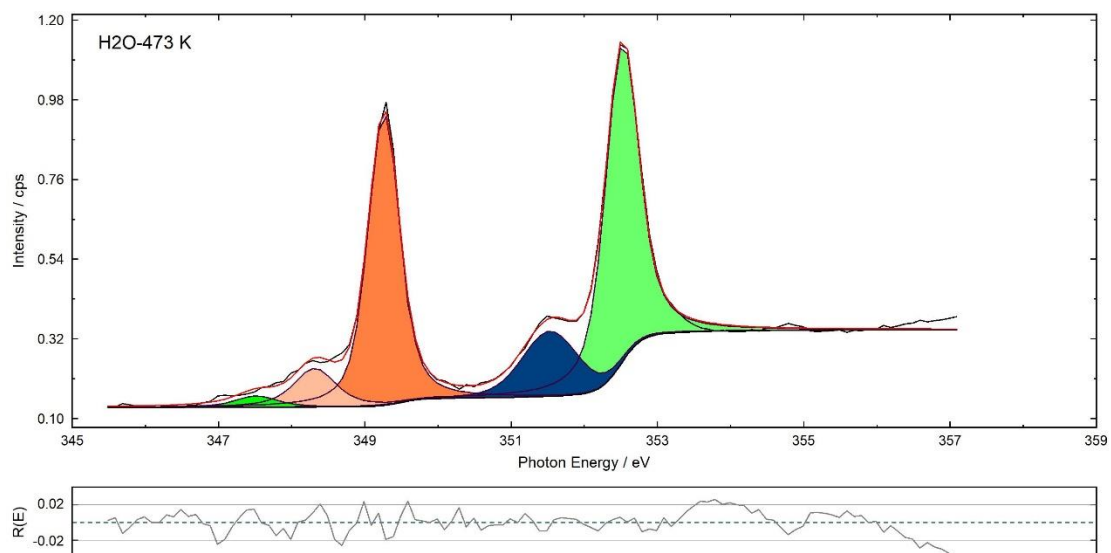


Figure S22. Ca  $L_{2,3}$ -edge NEXAFS spectra of amorphous calcium carbonate acquired at 473 K under an atmosphere of 0.4 mbar of water vapor.

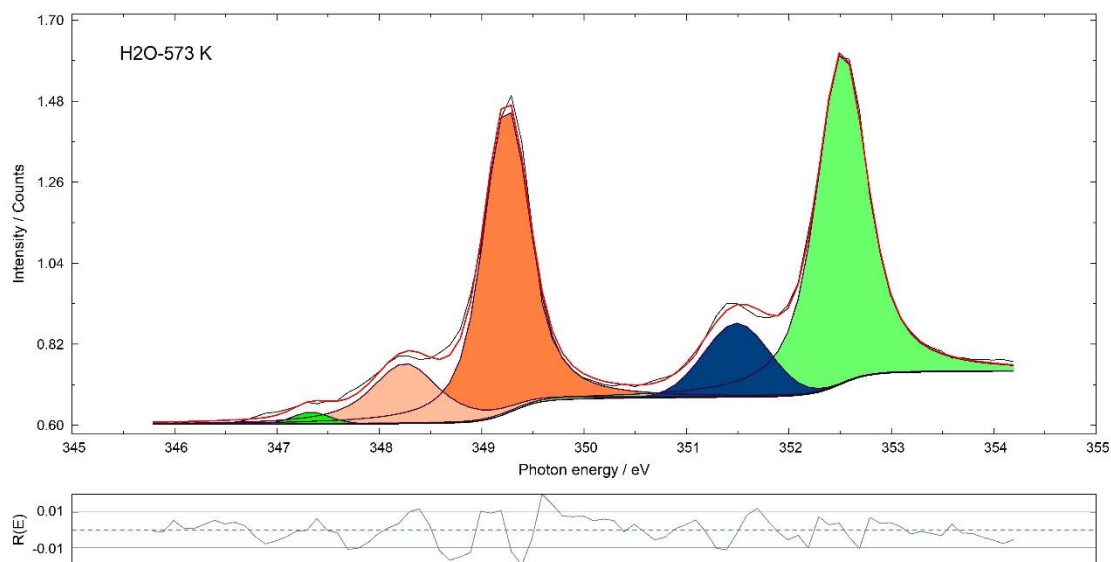


Figure S23. Ca  $L_{2,3}$ -edge NEXAFS spectra of amorphous calcium carbonate acquired at 573 K under an atmosphere of 0.4 mbar of water vapor.

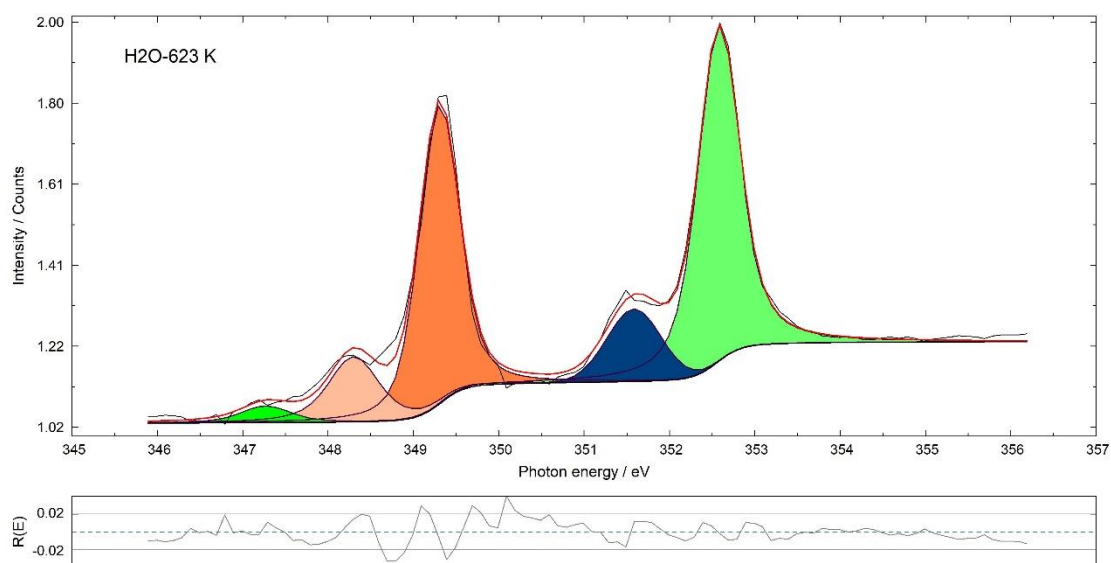


Figure S24. Ca  $L_{2,3}$ -edge NEXAFS spectra of amorphous calcium carbonate acquired at 623 K under an atmosphere of 0.4 mbar of water vapor.

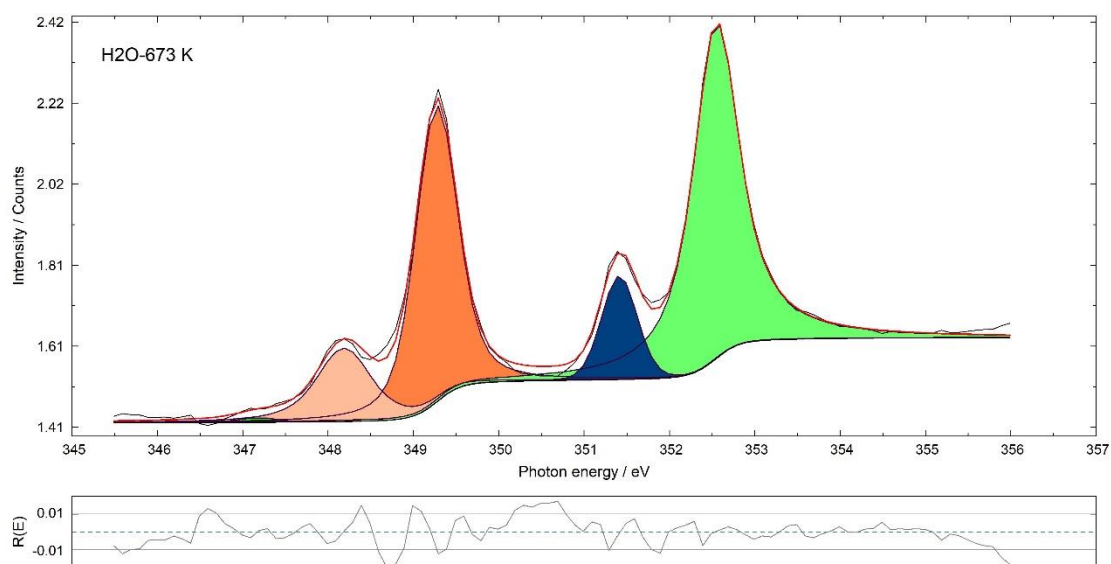


Figure S25. Ca  $L_{2,3}$ -edge NEXAFS spectra of amorphous calcium carbonate acquired at 673 K under an atmosphere of 0.4 mbar of water vapor.

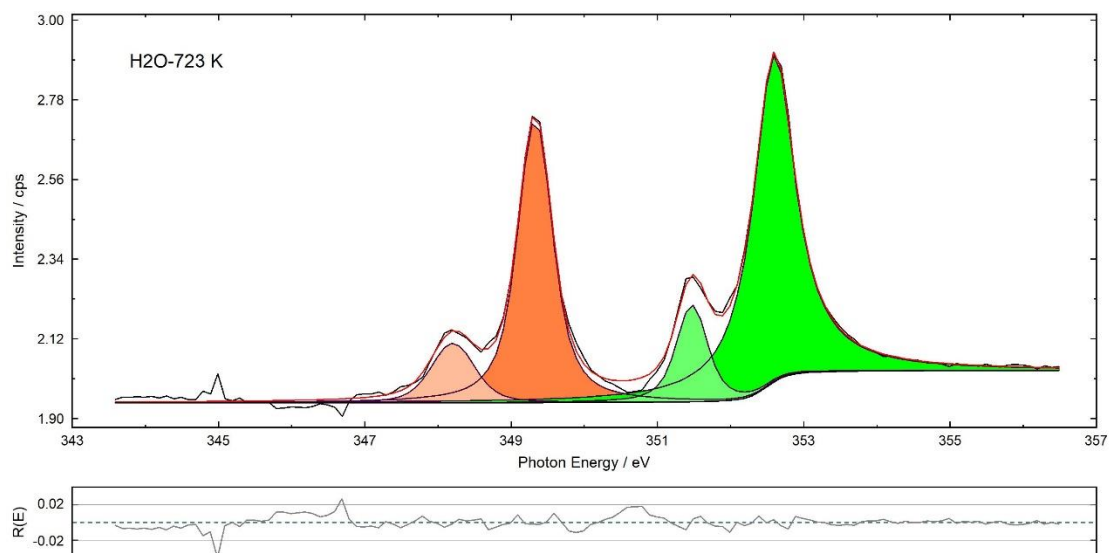


Figure S26. Ca  $L_{2,3}$ -edge NEXAFS spectra of amorphous calcium carbonate acquired at 723 K under an atmosphere of 0.4 mbar of water vapor.

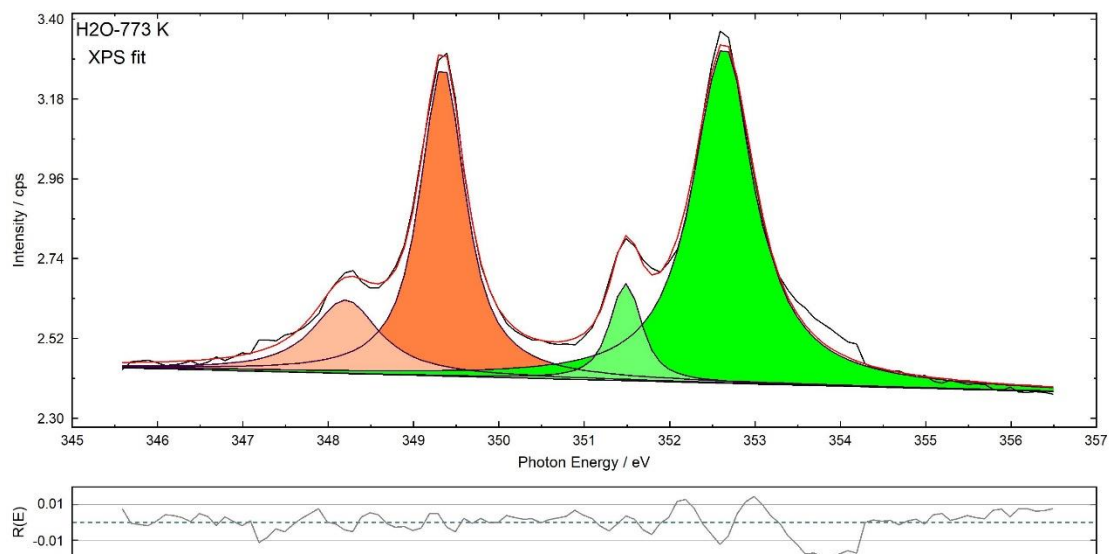


Figure S27. Ca  $L_{2,3}$ -edge NEXAFS spectra of amorphous calcium carbonate acquired at 773 K under an atmosphere of 0.4 mbar of water vapor.

**Table S1.** Summary of the spectral parameters extracted from the Ca *L*-edge NEXAFS spectra of the calcite samples at room temperature.

		<b>Commercial</b>	<b>Direct Mixing</b>
<b>Peak 1</b>	Position (eV)	352.56	352.52
	GP-FWHM (eV)	0.35	0.34
	LP-FWHM (eV)	0.33	0.23
<b>Peak 2</b>	Position (eV)	351.45	351.29
	GP-FWHM (eV)	0.35	0.26
	LP-FWHM (eV)	0.40	0.19
<b>Peak 3</b>	Position (eV)	349.28	349.20
	GP-FWHM (eV)	0.35	0.28
	LP-FWHM (eV)	0.20	0.22
<b>Peak 4</b>	Position (eV)	348.21	347.97
	GP-FWHM (eV)	0.28	0.35
	LP-FWHM (eV)	0.59	0.13
<b>Peak 5</b>	Position (eV)	347.12	--
	GP-FWHM (eV)	0.31	--
	LP-FWHM (eV)	0.26	--
L <sub>2</sub> splitting (eV)		1.11	1.23
L <sub>3</sub> splitting (eV)		1.07	1.23

**Table S2.** Results of Rietveld analysis of the powder XRD diffractograms of the calcite samples.

Sample	wR	$R_{F2}$	Residual Fourier Map ( $\Delta F$ )			Size of crystalline domain
			max	min	sigma	
Commercial Calcite	6.81%	5.41%	0.749	-0.358	0.107	129 nm
Synthetic Calcite	8.64%	4.41%	0.400	-0.261	0.100	10 $\mu$ m

**Table S3.** Structural parameters extracted from the Rietveld analysis.

Sample	Atom	Fractional coordinates			Occupancy	$U_{iso}$
Commercial calcite	Ca	0.0	0.0	0.0	1.0	0.0230 (9)
	C	0.0	0.0	0.25	1.0	0.0230 (9)
	O	0.2577 (1)	0.0	0.25	1.0	0.0230 (9)
Synthetic calcite	Ca	0.0	0.0	0.0	1.0	0.0091 (8)
	C	0.0	0.0	0.25	1.0	0.0091 (8)
	O	0.2579 (1)	0.0	0.25	1.0	0.0091 (8)

**Table S4.** Summary of the spectral parameters extracted for the Ca  $L_{2,3}$ -edge NEXAFS measurements carried out for ACC samples under UHV conditions.

		<b>300 K</b>	<b>373 K</b>	<b>403 K</b>	<b>473 K</b>	<b>523 K</b>	<b>573 K</b>
<b>Peak 1</b>	Position (eV)	352.56	352.57	352.56	352.59	352.55	352.52
	GP-FWHM (eV)	0.45	0.46	0.3	0.37	0.38	0.36
	LP-FWHM (eV)	0.43	0.42	0.67	0.58	0.60	0.60
<b>Peak 2</b>	Position (eV)	351.56	351.56	351.53	351.62	351.59	351.62
	GP-FWHM (eV)	0.52	0.49	0.44	0.53	0.56	0.54
	LP-FWHM (eV)	0.26	0.33	0.32	0.25	0.23	0.23
<b>Peak 3</b>	Position (eV)	349.30	349.30	349.32	349.33	349.30	349.28
	GP-FWHM (eV)	0.46	0.46	0.38	0.53	0.49	0.50
	LP-FWHM (eV)	0.31	0.31	0.40	0.23	0.30	0.29
<b>Peak 4</b>	Position (eV)	348.40	348.40	348.42	348.47	348.50	348.51
	GP-FWHM (eV)	0.46	0.46	0.36	0.53	0.49	0.50
	LP-FWHM (eV)	0.63	0.63	0.75	0.46	0.60	0.53
<b>Peak 5</b>	Position (eV)	347.66	347.66	347.50	347.64	347.58	347.87
	GP-FWHM (eV)	0.46	0.46	0.36	0.53	0.49	0.50
	LP-FWHM (eV)	0.63	0.63	0.74	0.44	0.60	0.42
<b>L2 splitting (eV)</b>		1.00	1.01	1.03	0.97	0.96	0.90
<b>L3 splitting (eV)</b>		0.90	0.90	0.90	0.86	0.80	0.77

**Table S4.** Continued.

		<b>623 K</b>	<b>673 K</b>	<b>723 K</b>	<b>773 K</b>
<b>Peak 1</b>	Position (eV)	352.59	352.55	352.53	352.48
	GP-FWHM (eV)	0.31	0.48	0.40	0.39
	LP-FWHM (eV)	0.71	0.50	0.71	0.71
<b>Peak 2</b>	Position (eV)	351.63	351.60	351.47	351.45
	GP-FWHM (eV)	0.59	0.59	0.44	0.53
	LP-FWHM (eV)	0.13	0.36	0.41	0.32
<b>Peak 3</b>	Position (eV)	349.34	349.29	349.26	349.21
	GP-FWHM (eV)	0.51	0.44	0.59	0.71
	LP-FWHM (eV)	0.32	0.38	0.29	0.17
<b>Peak 4</b>	Position (eV)	348.47	348.42	348.26	348.21
	GP-FWHM (eV)	0.51	0.44	0.59	0.61
	LP-FWHM (eV)	0.65	0.77	0.29	0.27
<b>Peak 5</b>	Position (eV)	347.55	347.37	347.37	347.25
	GP-FWHM (eV)	0.51	0.44	0.59	0.61
	LP-FWHM (eV)	0.40	0.70	0.29	0.27
<b>L<sub>2</sub> splitting (eV)</b>		0.96	0.95	1.06	1.03
<b>L<sub>3</sub> splitting (eV)</b>		0.87	0.87	1.00	1.00

**Table S5.** Summary of the spectral parameters extracted for the Ca  $L_{2,3}$ -edge NEXAFS measurements carried out for ACC samples under an atmosphere of 0.4 mbar of water vapor (relative humidity of 1.3%).

		<b>300 K</b>	<b>373 K</b>	<b>473 K</b>	<b>573 K</b>	<b>623 K</b>	<b>673 K</b>
<b>Peak 1</b>	Position (eV)	352.54	352.54	352.51	352.52	352.58	352.55
	GP-FWHM (eV)	0.29	0.30	0.38	0.35	0.41	0.36
	LP-FWHM (eV)	0.38	0.38	0.28	0.38	0.29	0.45
<b>Peak 2</b>	Position (eV)	351.52	351.54	351.49	351.48	351.57	351.43
	GP-FWHM (eV)	0.40	0.40	0.67	0.37	0.45	0.46
	LP-FWHM (eV)	0.20	0.20	0.25	0.44	0.32	0.32
<b>Peak 3</b>	Position (eV)	349.28	349.27	349.26	349.24	349.30	349.27
	GP-FWHM (eV)	0.34	0.39	0.37	0.35	0.45	0.44
	LP-FWHM (eV)	0.23	0.19	0.23	0.30	0.20	0.24
<b>Peak 4</b>	Position (eV)	348.43	348.48	348.35	348.25	348.30	348.19
	GP-FWHM (eV)	0.32	0.39	0.37	0.35	0.45	0.44
	LP-FWHM (eV)	0.51	0.38	0.45	0.60	0.40	0.48
<b>Peak 5</b>	Position (eV)	347.71	347.98	347.67	347.34	347.27	347.17
	GP-FWHM (eV)	0.32	0.39	0.37	0.35	0.45	0.34
	LP-FWHM (eV)	0.51	0.38	0.45	0.32	0.40	0.29
<b>L<sub>2</sub> splitting (eV)</b>		1.02	1.00	1.02	1.04	1.01	1.12
<b>L<sub>3</sub> splitting (eV)</b>		0.85	0.79	0.91	0.99	1.00	1.08

**Table S5.** Continued.<sup>1</sup>

		<b>723 K</b>	<b>773 K</b>
<b>Peak 1</b>	Position (eV)	352.60	352.63
	GP-FWHM (eV)	0.14	0.21
	LP-FWHM (eV)	0.68	0.83
<b>Peak 2</b>	Position (eV)	351.46	351.48
	GP-FWHM (eV)	0.32	0.21
	LP-FWHM (eV)	0.29	0.34
<b>Peak 3</b>	Position (eV)	349.32	349.34
	GP-FWHM (eV)	0.29	0.21
	LP-FWHM (eV)	0.41	0.56
<b>Peak 4</b>	Position (eV)	348.23	348.20
	GP-FWHM (eV)	0.41	0.21
	LP-FWHM (eV)	0.38	0.88
<b>L<sub>2</sub> splitting (eV)</b>		1.14	1.15
<b>L<sub>3</sub> splitting (eV)</b>		1.09	1.14

<sup>1</sup> Only four components were required to obtain a good fit to the data.

## References

- [1] B. H. Toby, R. B. Von Dreele, *J. Appl. Crystallogr.* **2013**, *46*, 544–549.
- [2] Y. Politi, R. A. Metzler, M. Abrecht, B. Gilbert, F. H. Wilt, I. Sagi, L. Addadi, S. Weiner, P. U. P. A. Gilbert, *Proc. Natl. Acad. Sci. U. S. A.* **2008**, *105*, 17362–17366.